OCCAM

OXFORD CENTRE FOR COLLABORATIVE APPLIED MATHEMATICS

A stochastic model for early placental development

by

Simon L. Cotter
Václav Klika
Laura S. Kimpton
Sally L. Collins
Alex E. P. Heazell

OCCAM Preprint Number 13/15

A Stochastic Model for Early Placental Development

By Simon L. Cotter[1,*], Václav Klika[2,3], Laura S. Kimpton[3], Sally L. Collins[4,5] and Alex E. P. Heazell[6,7] on behalf of the Mathematics in Medicine Study Group on Placental Shape and Structure

[1]*School of Mathematics, University of Manchester, Oxford Road, Manchester, UK*
[2]*Department of Mathematics, FNSPE, Czech Technical University in Prague, Trojanova 13, Prague 2, 120 00, Czech Republic*
[3]*Mathematical Institute, University of Oxford, 24-29 St. Giles, Oxford, UK*
[4]*The Nuffield Department of Obstetrics & Gynaecology, University of Oxford, Oxford, UK*
[5]*The Fetal Medicine Unit, John Radcliffe Hospital, Oxford, UK*
[6]*Institute of Human Development, Maternal and Fetal Health Research Centre, University of Manchester, Manchester, UK*
[7]*Maternal and Fetal Health Research Centre, St. Mary's Hospital, Central Manchester University Hospitals NHS Foundation Trust, Manchester Academic Health Science Centre, Manchester, UK*

In the human, placental structure is closely related to placental function and consequent pregnancy outcome. Studies have noted abnormal placental shape in small-for-gestational age infants which extends to increased lifetime risk of cardiovascular disease. The origins and determinants of placental shape are incompletely understood and are difficult to study in vivo. In this paper we model the early development of the placenta in the human, based on the hypothesis that this is driven by dynamics dominated by a chemo-attractant effect emanating from proximal spiral arteries in the decidua. We derive and explore a two-dimensional stochastic model for these events, and investigate the effects of loss of spiral arteries in regions near to the cord insertion on the shape of the placenta. This model demonstrates that placental shape is highly variable and disruption of spiral arteries can exert profound effects on placental shape, particularly if this disruption is close to the cord insertion. Thus, placental shape reflects the underlying maternal vascular bed. Abnormal placental shape may reflect an abnormal uterine environment, which predisposes to pregnancy complications.

Keywords: Mathematical modelling; Placental development; Placental shape; Spiral artery; Stochastic dynamics.

1. Introduction

Pregnancy outcome is fundamentally dependent on placental function, which is itself closely related to placental shape and structure. Epidemiological data suggest that alterations of placental shape are increased in small for gestational age

*Corresponding author (simon.cotter@manchester.ac.uk)

pregnancies[23] which extends to increased lifetime risk of hypertension and coronary heart disease[1, 11]. Placental shape is hypothesised to be determined in early pregnancy when the chorion, which covers the spherical embryo in three dimensions, regresses to form the chorion laeve and the placenta[29]. The underlying determinants of the relationship between placental shape and function are not fully understood.

In common with other events occuring in early to mid pregnancy, determination of placental shape is difficult to study in vivo and ex vivo due to the limits of imaging, availability of tissue and if tissue is obtained, the ultimate outcome of the pregnancy remains unknown. To address these difficulties, several groups have applied mathematical modelling techniques to the placenta including: oxygen transfer across the villus[8], development of placental shape[37], and fetoplacental blood flow[16]. With relevance to placental shape, Yampolsky et al. used a Diffusion Limited Aggregation (DLA) model to general placental vascular trees[37]. Using this model different shapes could be generated. However, this model was not influenced by the environment in which the placenta develops. We hypothesised that placental shape is determined by the uterine environment in early pregnancy. To address this hypothesis we aimed to develop a mathematical model which included entry of nutrients/oxygen from the maternal epithelium during early placental villous development and subsequent vascularisation. We then aimed to run this model to determine the effects of changing the maternal environment on placental shape.

2. Placental growth model

We assume that placental villous development and subsequent angiogenesis is a chemotactically driven process, with the attracting chemical X being maximally available to growing placental tissue once it reaches the opening of a spiral artery; potential chemoattractant(s) released from maternal spiral arteries include oxygen, growth factors, cytokines or nutrients[28]. However, we assume in this paper that the most relevant factor is oxygen as this is known to be a potent regulator of angiogenesis explored in other in silico models[34].

(*a*) *Dynamics of the fetal villous tips*

We model the growth of the tips of the fetal villous tree by a stochastic differential equation. We assume that the direction of growth of the tips is dominated by the chemoattractant emanating from the maternal spiral arteries, which are fixed points in the decidua. Since the villous tip's observation of the gradient of the chemoattractant is likely to be noisy, we model this through the addition of Brownian motion to the trajectory. Therefore, the villous tip $\mathbf{x}_p \in \mathbb{R}^2$ is acting in an evolving potential $V(\mathbf{x}, t)$, due to the concentration of chemoattractant.

The potential itself is evolving for two reasons. The first is that we assume that the villous tips are themselves sinks for the chemoattractant, at a rate comparable to that of an activated spiral artery. Since all the other villous tips in the system are moving, the potential function itself is constantly changing. The second is that we assume that all the spiral arteries are initially "switched off". A spiral artery only becomes "switched on" if a fetal villous tip comes within a given radius of that artery. We assume that within this radius, the trophoblasts emanating from

the placenta will reach the spiral artery and prepare it for inclusion in the maternal uteroplacental vascular network[24]. Once this has happened, we assume that the spiral artery has become a source of the chemoattractant. We will describe the exact form of the potential function $V(\mathbf{x}, t)$ in Section 3.

Taking into account the effect of the chemoattractant potential field V, and the noisy observation of this potential field by the villous tip, we arrive at the following stochastic differential equation for the evolution of the position of the villous tip:

$$\mathrm{d}\mathbf{x}_p = -\nabla V(\mathbf{x}_p, t) + \sigma \mathrm{d}\mathbf{B}. \tag{2.1}$$

Here $\mathbf{B}$ is a two-dimensional Brownian motion, and σ is the standard deviation of the noise in the trajectory of the villous tip, due to noisy observations of the chemoattractant gradient. Note that trajectories of this system are attracted to regions where is the lowest (or even negative).Trajectories of this form can be discretised by use of the Euler-Marayama scheme, which, for a time step of size Δt, is given by the following expression:

$$\mathbf{x}_p((n+1)\Delta t) = \mathbf{x}_p(n\Delta t) - \Delta t \nabla V(\mathbf{x}_p(n\Delta t), n\Delta t) + \sigma\sqrt{\Delta t}\xi_n, \qquad \xi_n \sim \mathcal{N}(0,1) \quad \text{i.i.d.} \tag{2.2}$$

We use this formula for the update of each of the fetal villous tips in the system, and record the history of the trajectories of each of the tips. The path of the tip represents the shape of the villous tree being grown. Higher order numerical methods exist for the solution of SDEs, such as the Milstein method[25], or stochastic analogues of higher order Runga-Kutte methods[21]. However, for our needs, the Euler-Marayama scheme is sufficient.

(*b*) *Branching of the fetal villous tree*

Based on knowledge of the potential field, we propose a branching condition for the growing tips of the fetal villous tree. Neglecting some corrections which will be given in more detail below, we assume that branching occurs when the gradient of the potential field has small absolute value at the point that the villous tip is occupying. Low gradient means poor information for the villous tip to decide in which direction it should grow. If the concentration of chemoattractant is simultaneously non-zero in this location, this small gradient will in general be due to the villous tip's path heading in a direction which would approximately perpendicularly bisect a line between two spiral arteries. In this situation it is advantageous for the villous tree to split in order to attach itself to both spiral arteries.

We also add further corrections to prevent branching near the cord insertion (where it is very likely that there will be several sources of chemoattractant of similar strength/distance), and also where the chemoattractant concentration is essentially zero in that local area, at the sources (except the initial stages of angiogenesis), or near another tip of a growing villous tip. Below we discuss all these conditions in more details.

We start with an initial number $N_0 = 2$ of growing tips from the point of insertion of the umbilical cord on the placental disc. The probability of branching per time unit is proposed to be in the following form:

$$P_{\text{split}} = \min\left\{1, \exp\left\{L\left(\frac{S}{\|\nabla V(\mathbf{x})\|} - 1\right)\right\}\right\}, \tag{2.3}$$

meaning that the flatter the potential field is (compared to the value of parameter S) at a given point $\mathbf{x}$, the (exponentially) more probable the branching is. The parameter L represents a likelihood constant of branching. A few corrections are needed though as the potential field contains contributions from sources (negative) and growing tips (positive). The considered corrections for branching probability at the growing tip $\mathbf{x}_p$ are the following:

- If $V(\mathbf{x}_p) > 0$ then $P_{\text{split}} = 0$. This condition represent a no-split requirement if the concentration of chemoattractant is essentially zero in that local area as $V(\mathbf{x}_p) > 0$ means that there is more consumption of the chemoattractant by the growing tips than is being produced by the sources in that area.

- If $\|\mathbf{x}_p\| < \varepsilon$ then $P_{\text{split}} = 0$, for some $0 < \epsilon \ll 1$. We prevent branching from happening when the tip $\mathbf{x}_p$ is close to the umbilical cord insertion as the gradient there can be expected to be low due to several sources of similar magnitude distributed around the insertion. In general, a large amount of branching of the villous tree at the cord insertion is not usually observed in real placentas.

- If distance to the nearest source is less than ε and the nearest source has not been reached yet by any growing villous tips then the probability is set to zero $P_{\text{split}} = 0$. Only in initial stages of angiogenesis we assume that branching occurs once a source is reached (until some number $N_{\text{ini}} = 6$ of sources is reached). Otherwise growing tips would quickly find some nearest sources without branching enough to enable a full villous tree with $N_T = 30$ terminations in sources to be grown.

- if distance to the nearest growing villous tip is less than ε we set the probability of branching to zero $P_{\text{split}} = 0$ to prevent multiple branching of the same villous tip in a very short time.

(c) *Activation of spiral arteries*

As described before, we assume that at the time when the embryo becomes attached to the decidua, the spiral arteries are not releasing significant amounts of the chemoattractant factors. They only become "switched on" when in close enough proximity to a villous tip, in order for the trophoblasts to invade the site[24]. Therefore, we define a parameter $R_{\text{troph}} > 0$. After updating the positions of the villous tips, all of the "switched off" spiral arteries are checked to see if there are any villous tips within a distance R_{troph} of them. If they are, then the spiral artery is "switched on", and its effect is added to the potential function for the next time step (see Section 3 for more details of the potential function).

A spiral artery only becomes inactive again if a villous tip is assumed to have terminated at this source, as we describe in the next subsection.

(d) *Stopping condition for villous tips*

As simulated angiogenesis is dimensionless, with one unit equal to a typical distance among spiral arteries (12 mm, see Section 3 (b)) we include this scaling in our potential field. Further, since both the potential and its gradient are growing

to infinity as the source is approached and since, as was mentioned above, in the vicinity of a source there are two villous tips that are actually growing towards each other (one from the maternal villous tree and one being the fetal villous tip itself), we stop the growth of a villous tip once it is closer than a certain threshold value D_{stop} to a source and consider it to have reached that source. At this point, we assume that the sink of the villous tip, and the source of the spiral artery cancel each other out, and both are turned off for the remainder of the simulation.

(*e*) *Stopping condition for the villous tree*

It has been observed that approximately 30, and no more than 50 spiral arteries, are connected to the average placenta (one per placental cotyledon). Therefore, we decided to choose a number of arteries N_T that are reached before the simulation finishes. As soon as this threshold has been reached, the growth of the villous tree is stopped, and any parts of the tree which have not yet reached a spiral artery are removed from the simulation (they have not found a source of nutrition and therefore will simply not develop into a fully functioning part of the villous network). In this model we assume that once this process is complete, all villi are subsequently vascularised, and then link up with the vascular tree developing on the chorionic plate.

3. Finding an appropriate potential field

We propose a potential field of the growth factor that a single spiral artery produces to correspond to a diffusion of a chemical from a point source with a magnitude M (neglecting the possible effects of spiral artery size) constant in time from its onset at time t_0. Thus the potential field $V(\mathbf{x}, t)$ is a solution of:

$$\frac{\partial}{\partial t}V(\mathbf{x},t) - \left(D\nabla^2 V(\mathbf{x},t) - k^2 V(\mathbf{x},t)\right) = M\delta(\mathbf{x}_0) \otimes \theta(t - t_0) \tag{3.1}$$

where consumption of the attracting chemical by surrounding tissue, with a rate k^2, is considered and $\theta(t)$ denotes a Heaviside function. Consumption of oxygen is more appropriately modelled by a Menten-Michaelis term instead of linear consumption but this dependence is rational when oxygen concentration is low: $\frac{M_0 P}{P_0+P} \approx \frac{M_0}{P_0}P$. The solution, in general, to this problem can be found by calculating Green's function (also called the fundamental solution) of the differential operator using Fourier transformation. However, the potential with its gradient (needed for chemotactic growth) cannot be rewritten into analytical or closed form which is desired for our purposes. That is why we will look for a steady state solution instead which essentially means that we assume the diffusion process of the attracting chemical X to be much faster compared to villous tree growth. It can be shown† that the stationary potential field $V(\mathbf{x})$ is proportional to the modified Bessel function and is given by:

$$V(r) = \frac{M}{2\pi}K_0\left(r\frac{k}{\sqrt{D}}\right) \tag{3.2}$$

with asymptotic behaviour $K_0(x) \approx -\ln(x/2) - \gamma,\ 0 < x \ll 1$.

† See supplementary file for derivation.

(a) *Initial distribution of the spiral arteries*

The initial distribution of the spiral arteries that we have implemented can be described by the following algorithm:

1. It is believed that there are roughly 200 spiral arteries in an average uterus. We take it to be exactly $N_{\text{sources}} = 200$. We assume that as the fetus grows, and the uterus distends that the distance between the spiral arteries increases in proportion to increase in placental size.

2. We randomly distribute this number of spiral arteries throughout the considered circular domain which we assume has radius $r_\Omega = \sqrt{(N_{\text{sources}})/\pi}$. Therefore, on average, there is one source per 1 unit squared.

3. Create random samples from the uniform distribution of sources on the circle, conditioned on no two sources being closer than $\rho_{\min} = 0.7$ to each other. Note that a uniform distribution on a circle is obtained by sampling $\theta = U([0, 2\pi])$, $r = r_\Omega\sqrt{U([0, 1])}$, and taking $\mathbf{x} = r\cos(\theta)$.

We hypothesise that disrupted placental shape may be related to blocked, damaged or missing spiral arteries in certain regions of the uterus. We also consider the effect of maldevelopment of the maternal vascular network leading to a whole region of blocked/switched off spiral arteries. Low and irregular densities of spiral arteries close to the point of adhesion of the embryo to the uterus can cause, as we show in Section 6, irregularly and bipartite shaped placentas, and off-centre cord insertions. This in itself may not be the cause of problems in pregnancy, but we hypothesise that it is certainly an indication of a poor or irregular blood supply to the placenta, and therefore to the fetus, which in turn could cause low birth weight.

The initial distribution of spiral arteries in simulations with disrupted scenarios are carried out in the same way as described above at first. Once a uterus has been stocked with 200 spiral arteries before, we then identify which of these lie within the region where sources (spiral arteries) are being blocked/switched off. We consider this region to be circular with a given radius r_{disrupt} and centre s_{disrupt} (WLOG to be on the x-axis). Any spiral arteries in this region are switched off, and not replaced anywhere else in the domain, leading in general to less than 200 healthy spiral arteries. For the simulation of bipartite placentas we hypothesise that this is caused by two disrupted regions which are symmetric with respect to the cord insertion.

(b) *Parameter estimation*

The overall potential landscape is a sum of point source contributions from each active spiral artery and growing tip. We consider exactly the same potential for a point source but with an opposite sign since we assume the growing tip to be a constant sink of attracting chemical. As there is not enough data to determine the magnitude of point sources of spiral arteries and compare them with sinks and with each other, we assume them to be of equal magnitude (so once a source is actually reached by a growing villous tip their potentials cancel out). To summarise, the

potential driving the chemotactical angiogenesis is

$$V(\mathbf{x}) = \sum_j \frac{M_j}{2\pi} K_0\left(s_j \frac{k}{\sqrt{D}}\right) - \sum_i \frac{M_i}{2\pi} K_0\left(r_i \frac{k}{\sqrt{D}}\right), \tag{3.3}$$

where the second summation is carried out over all sources i with magnitudes M_i and r_i being the distance from the given point ($\mathbf{x}$) to a source i. Similarly the first summation is carried out over all current non-terminated villous tips with magnitudes M_j and s_j being the distance from the given point ($\mathbf{x}$) to a villous tip j. Magnitudes of all sources and sinks were considered to be equal, $M_i = 1,\ \forall i$ and $M_j = 1,\ \forall j$. Notice that there is essentially only a single parameter $\frac{k}{\sqrt{D}}$ which needs to be determined.

A relevant value for the consumption rate of oxygen in placental tissue was calculated from *in vitro* data to be $4.96 \frac{mmol\ \mathrm{O_2}}{\mathrm{m^3\ tissue}}$/s[4]. This leads to a value of $k = \frac{32}{1.429} \times 4.96 \times 10^{-3} = 0.11 \times 10^{-3}$[1/s]. Diffusion coefficient in the endometrium is $D = 5.5 \times 10^{-10}$m/s [19]. Thus the single model parameter can be estimated to be $\frac{k}{\sqrt{D}} = 4.69$.

The last task is to estimate the actual distance between spiral arteries in the placenta in this considered phase of the villous tree development. There is a consensus that there are roughly 200 spiral arteries in the whole uterus. The three dimensions of the uterus have been measured in both nulliparous and multiparous women. Uteral mean size is measured from three quantities: Length is measured from the fundus to the external os, the anterposterior diameter is the maximum length in the midsgittal section of the body of the uterus in the anterposterior direction, and uterine width is the maximum measurement obtained in a cross-section of the fundus.

Let us assume for simplicity that the uterus is of ellipsoidal shape in early stages of pregnancy. The formula used to compute the surface area of an ellipsoid is an approximation known as Knud Thomsons formula with p=1.6075[20]:

$$\text{area} \approx 4\pi \left(\frac{a^p b^p + a^p c^p + b^p c^p}{3}\right)^{1/p} \text{mm}^2.$$

The mean values reported in literature vary (e.g. [12, 7, 2, 30, 36]), but they all lead to estimation of distance 12-13 mm between spiral arteries, where we have used the above mentioned Knud Thomson's formula. We shall consider the mean uterus size to be 75.0 mm 25.0 mm 50.0 mm [36], with the estimate of 12 mm being the average distance between spiral arteries.

4. Estimating placental shape

To estimate the shape of a given placenta based on its villous tree, we use the following approach. Given a point in space (in the plane) we simply ask wether it is inside the considered placenta or not. We count a sum of weighted distances of the considered point to each segment (of a given length) of the villous tree and if it is less than a certain threshold value σ_{thresh}, we regard the considered point to be within the placenta. This choice is motivated by diffusion from the vascular network, where we assume that concentration of a chemical from a constant source

Table 1. *List of parameters*

Parameter value	**Meaning**
$\Delta t = 10^{-3}$	considered time step in villous tree growth
$L = 0.1$	likelihood constant of branching
$S = 0.5$	branching level
$\varepsilon = 10^{-2}$	used in corrections of probability branching condition
$D_{\text{stop}} = 10^{-2}$	threshold value for stopping near sources
$R_{\text{troph}} = 1.5$	radius of effect of trophoblasts from villous tips
$N_0 = 2$	initial number of growing tips from cord
$N_{\text{ini}} = 6$	initial phase of angiogenesis when we consider a split to occur each time a source is reached (until N_{ini} sources were reached)
$N_T = 30$	number of arteries that are reached before the simulation finishes
$\rho = 5$	a scaling constant used for finding suitable resolution/magnitude of "an oxygen supply for placenta tissue from its vascular network"
$\sigma_{\text{thresh}} = 0.001$	threshold value for obtaining placental shape

decays with distance x as a modified Bessel function of the second kind $K_0(x)$ (see section 3). We also assume that a tissue (at the considered point) can survive only once it has access to a certain necessary (or minimal) amount of oxygen. Then to calculate what the level of oxygen is at the given point we need to sum the contributions from the whole vascular network, as we consider it to be the only source of oxygen. To summarise

$$\mathbf{x} \in \text{placenta} \Leftrightarrow OxLevel(\mathbf{x}) := \sum_{\text{segment}_i \in \text{vasculartree}} K_0\left(\rho(\text{dist}(\mathbf{x}, \text{segment}_i))\right) \geq \sigma_{\text{thresh}}.$$

The scaling constant ρ is used for finding suitable resolution/magnitude of "an oxygen supply for placenta from its vascular network", see Fig 1b,c. The length of all segments is the same and chosen to be 0.05 and the threshold value was set to $\sigma_{\text{thresh}} = 0.001$ which is used for obtaining a contour of the placenta, see Fig 1d.

5. Visualisation of the placenta

In this section we will describe how we visualise the output of the model as described in the previous sections. In the visualisation of the output of the model we had two aims.

- To create images of the vascular tree which were as realistic as possible, in order to visually compare them with the vascular trees of real placentas.
- To create images from the output of the model to indicate the shape of the placenta, and the position of the cord insertion, in order that we can apply the statistical measures as described in the sister paper to this work[17].

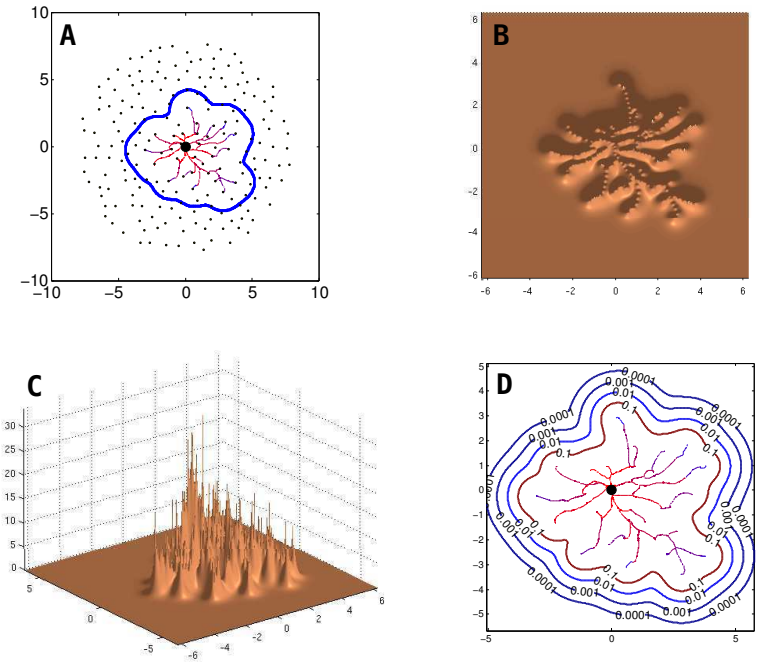

Figure 1. An example of shape estimation from an landscape of oxygen supply for placenta from its vascular network. **a)** A given network generated by the presented algorithm together with placental shape estimation. **b,c)** Plot of $OxLevel(\mathbf{x})$ function. **d)** Contour plot of $OxLevel(\mathbf{x})$ function for several values of σ_{thresh}.

The second objective is easily achieved, simply by plotting a circle at the point of cord insertion, an outline of the placental tissue, and a scale bar. See Figure 2.

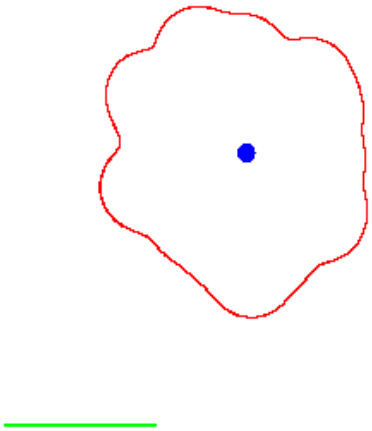

Figure 2. An example of the output of the model for analysis of the shape and cord insertion position of the placenta.

To achieve a more realistic look for the plotting of the vascularised villous tree, we also wanted to visualise the relative thickness of the branches of the villous tree. When two villous branches meet to form one larger branch, we can make an assumption about the relative thicknesses of the branches based on Murray's law[33]. Therefore, given a pair of branches with widths $w_1, w_2 > 0$ respectively, the combined branch where they join will be of width

$$w_3 = (w_1^3 + w_2^3)^{1/3}. \tag{5.1}$$

Once we have the villous tree, we first assign widths to each of the villous tips present at the end of the simulation that have terminated at a spiral artery. This width is based on the number of villous tips n which have terminated at the same spiral artery. Usually this will be just one, but on occasion two or more branches can find their way to the same spiral artery. Given that we assume that each spiral artery has width equal to 1 (non-dimensionalised width), we can assume that each of the emanating villous branches has width

$$w = n^{-1/3}.$$

Iterating back down the tree using the relation (5.1), we can assign realistic relative widths to all of the villous tree. We can then add this detail to our plot, to achieve pictures such as shown in the following section.

6. Numerical Results

In this section, we show results of the above presented model for placental vascular tree growth together with shape estimation. Three qualitatively different scenarios were considered. They differ only in the initial distribution of spiral arteries as described in section a. *Control* case corresponds to 200 available spiral arteries representing an "healthy" individual with none of the spiral arteries blocked. In the *disrupted* scenario, a circular region with a radius $r_{\text{disrupt}} = \sqrt{10/\pi} \approx 1.8$ and centre $s_{\text{disrupt}} = 0.5 + r_{\text{disrupt}} \approx 2.3$ has been blocked. This size of the radius means that on average 10 spiral arteries are blocked. The last considered case was *bipartite* case where two symmetrically positioned regions were considered having the same size and distance from the cord insertion as in the disrupted scenario. Typical plots in these three cases are given in Fig 3. Of course, the blocking of spiral arteries will have an impact almost only when a region *close* to the attachment of the umbilical cord is affected. This is because diffusion of attractor from spiral arteries (the shape of potential field) is considered to be the main driving force of angiogenesis in placenta.

Particular realisations of the presented stochastic model are not of interest here because of the indeterminism involved in each example. To draw qualitative conclusions/predictions from the model, we need to statistically analyse a large set of data. For this purpose we simulated the formation of 10,000 placentas in each scenario, and calculated statistical measures as proposed in our sister paper[17] using techniques described in Section 5 to extract umbilical cord placement within placenta, outer shape of placenta and scale bar. Only these results (plotted in Fig 4) can be compared to clinical data (ideally again a large set of data). The typical examples shown in Fig 3 show expected behaviour.

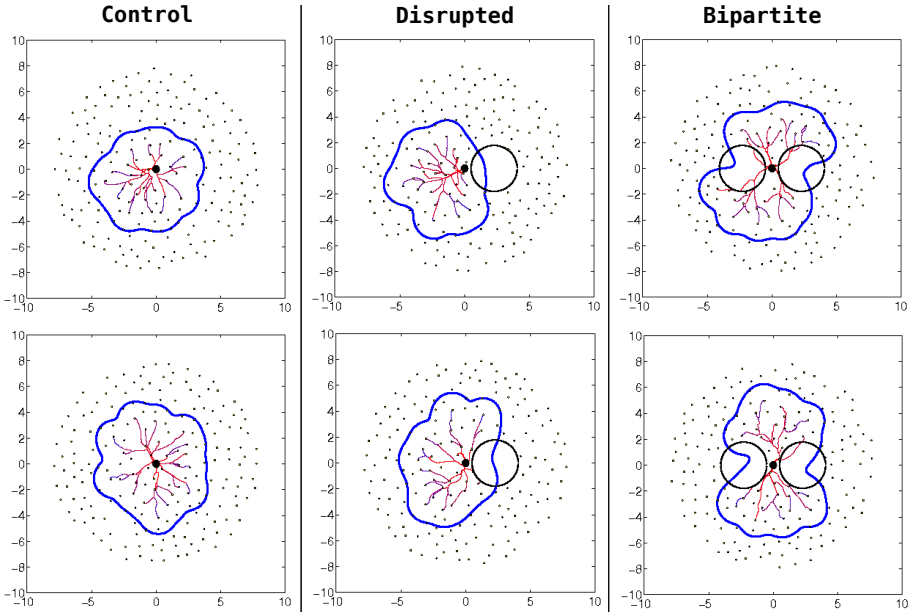

Figure 3. Examples of typical vascular tree predictions in the considered scenarios: control, disrupted (10 arteries blocked), bipartite (20 arteries blocked symmetrically according to cord insertion. The spiral arteries are depicted as black dots, blocked region by a black circle, vascular tree is plotted in blue-red colour and estimated placental shape by a blue thick solid line.

The used measures have roughly the following meaning (for more detailed descriptions see our sister paper[17]: α quantifies how central the cord insertion is, β is a measure of circularity ($\beta = 0$ for a circle), λ is the aspect ratio of longer to shorter axis from ellipticity, and we also measure the area of each placenta. These measures might enable us to estimate with a reasonably high probability to which scenario a given placenta most probably corresponds.

Notice that centrality corresponds well to control placentas as the average value together with magnitude of variations is clearly the lowest for the undisrupted control case. Placental area increases with the severity of disruptions and is likely to be related to necessity for the placenta to reach a given number of sources of growth factor (spiral arteries). Control placentas are the most circular ones, with the bipartite placentas the least circular. Circularity seems to be a better measure to distinguish between disrupted and bipartite case which is intuitive. Finally, the aspect ratio confirms that control placentas are the most round, and furthermore can be used to further distinguish between the disrupted and bipartite scenarios.

Let us consider a set of six randomly chosen placentas (two from each scenario) as generated by the presented model, see Fig. 5, and let us use the statistical results from our model to estimate to which scenario a given placenta belongs. It serves as a demonstration of the applicability of the presented model together with the proposed measures but also as a confirmation.

For example, consider two placenta from Fig 5 with values $\alpha = 0.129$, $\beta = 0.169$, $\lambda = 1.082$, $area = 63.1$ (fig A) and $\alpha = 0.26$, $\beta = 0.2$, $\lambda = 1.217$, $area = 56.27$ (fig B). Then we can estimate the probability of each measure that the con-

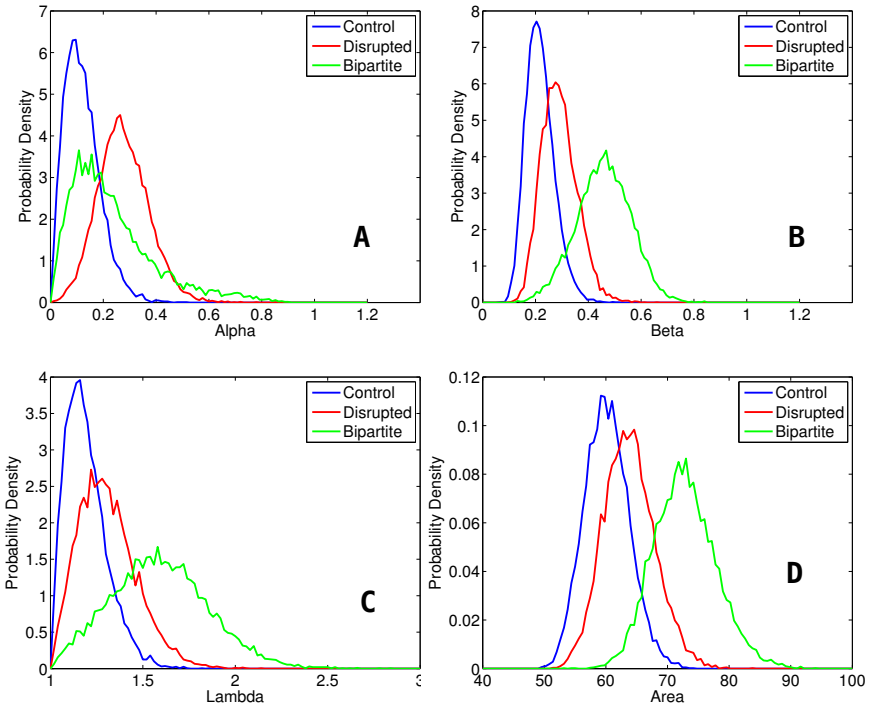

Figure 4. Probability density of proposed measures based on 10,000 simulations of the presented model for placental vascular tree and shape development. See the text for description of the measures.

sidered placenta corresponds to control, disrupted or bipartite case by calculating the integral of probability density functions in all cases over a 2% neighbourhood of the measure relevant scale (see Fig 6). Finally, by comparing these values we arrive at probabilities that the considered placenta corresponds to one of the three cases. Percentages are given in Table 2. Note that we obtain correct estimate for every example of placenta.

7. Discussion

Due to the inaccessibility of the placenta during pregnancy mathematical models have recently been utilised to study several aspects of placental physiology including amino acid transport[32], placental shape[37], oxygen transfer across the villus[14], blood flow through the fetal circulation[15, 22] and blood flow through the maternal component of the intervillous space[9]. In addition, models have explored pathological states including: fetal blood flow in hypertension[22], abnormal fetal blood flow in twin-twin transfusion syndrome[35] and reduced intervillous perfusion[31]. In these situations mathematical models have the advantages that they can be based on ex vivo and in vitro experimental data and, if they include biological variation, can be run many times to reproduce many individual pregnancies.

Here we developed a model of early placental development based upon data regarding the number of spiral arteries in the uterus and within the placental bed,

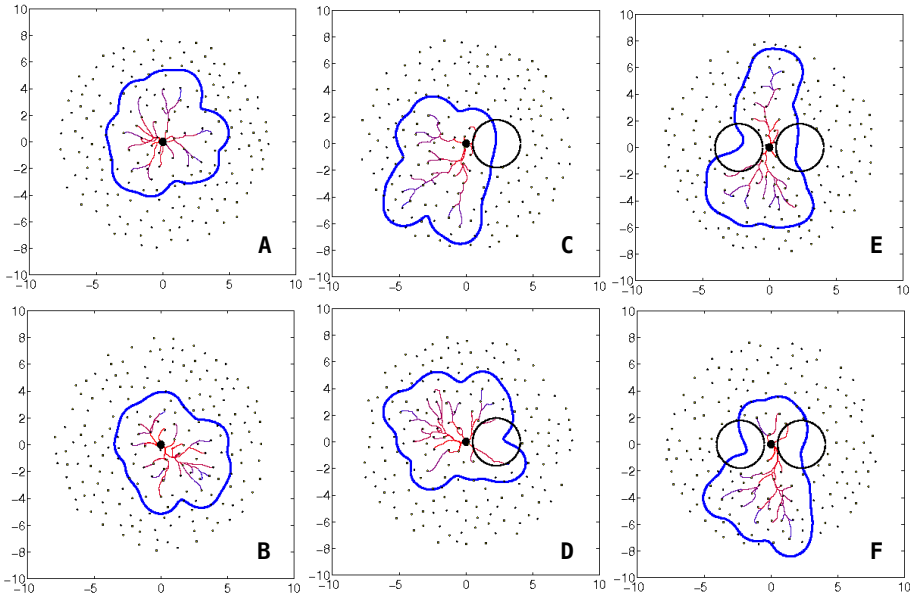

Figure 5. Six randomly chosen examples of placentas were used to estimate their relevance to each scenario using the proposed statistical measures. They are in fact particular realisations of control (the first column), disrupted (the second column), and bipartite (the third column) group.

the oxygen consumption of placental tissue and the diffusion of oxygen within the endometrium. We aimed to test the hypothesis that placental size or shape was closely related to presence and distribution of spiral arteries in the vicinity of placental development. Combined with objective measurements of placental shape our model suggests that there is significant variation in normal placental shape with a normal distribution for circularity, ellipticity, aspect ratio and cord insertion; with few placentas being perfectly discoid with a central cord insertion. These findings are identical to descriptions of placental shape and cord insertion in a cohort study of 861 infants which lends biological validity to our model[27]. Disruption of the normal field of spiral arteries significantly alters placental shape, resulting in a greater frequency of lateral cord insertion and bipartite placentas. This observation supports the hypothesis that maternal vascular bed determines placental shape to some extent. Thus, the abnormal placental shape, cord insertion and reduced placental area observed in small for gestational age infants may result from an abnormal uterine environment [6, 5], rather than abnormal placental shape being an independent determinant of fetal growth.

The strengths of this model include that it is based on ex vivo and in vitro observations and it has a random component which mimics biological variation assessed by formulae which have been successfully been used to evaluate placentas from normal pregnancies and those with small for gestational age infants[17]. In addition, this model was developed by a multidisciplinary team, providing biological, clinical and mathematical input. However, as with all mathematical models there are limitations. This model assumes that all nutrients, growth factors or oxygen will emanate from the same point source and have similar chemoattractant properties.

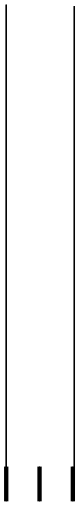

Figure 6. An illustration of probability estimation based on the surface underneath probability distribution function in each scenario (note that regions do overlap).

Some observations, particularly about the number of spiral arteries in a human uterus and placental bed, are from experiments performed over 50 years ago, but these would be almost impossible to repeat due to technical and ethical issues. Nevertheless, these estimates form the basis of modern understanding of uterine anatomy and changes in spiral arteries in early pregnancy.

There has been one other published study using a mathematical model to derive placental shape from early pregnancy events. Yampolsky et al. use a diffusion limited aggregation (DLA) tree to model the development of fetal vascular tree, on which placental shape is superimposed[37]. These images were compared with images of placental vascular trees and placental shape related to fetal weight via a metabolic scaling law[29]. This model also found that non-central cord insertion was associated with lower birthweight infants [38]. Although this model produces vascular trees which are reminiscent of the vascularisation of the chorionic plate, it is based on random growth of the vascular tree from a central point (the putative umbilical cord insertion); critically this assumes that feto-placental vascularisation determines placental shape. However, placental vascularisation is thought to be a secondary event occurring within the formed placental villi, with vessels growing out from the umbilical cord insertion, meeting vessels developing within stem villi [26]. Our model suggests that where there are no maternal spiral arteries, there is a reduction in trophic factors, villi do not develop and there is no subsequent feto-placental vascularisation. Thus, placental shape and the pattern of vessels on the chorionic plate is not a random event, but determined by the pattern of maternal spiral arteries.

Table 2. *Probabilities of correspondence of placentas from Fig. 5 to each scenario*

Fig A	control	disr.	bipart	**Fig B**	control	disr	bipart
$\alpha = 0.129$	53%	14%	33%	$\alpha = 0.26$	11%	59%	30%
$\beta = 0.169$	83%	16%	1%	$\beta = 0.2$	71%	27%	2%
$\lambda = 1.082$	69%	25%	6%	$\lambda = 1.217$	50%	40%	10%
$area = 63.1$	42%	52%	6%	$area = 56.3$	79%	21%	0%
avg	**61.75%**	26.75%	11.25%	**avg**	**52.75%**	36.75%	10.5%
Fig C	control	disr.	bipart	**Fig D**	control	disr	bipart
$\alpha = 0.567$	0%	22%	78%	$\alpha = 0.257$	12%	58%	30%
$\beta = 0.311$	20%	63%	17%	$\beta = 0.256$	44%	50%	6%
$\lambda = 1.338$	27%	51%	22%	$\lambda = 1.193$	54%	37%	9%
$area = 67.08$	14%	50%	36%	$area = 67.85$	11%	45%	44%
avg	15.25%	**46.5%**	38.25%	**avg**	30.25%	**47.5**%	22.25%
Fig E	control	disr.	bipart	**Fig F**	control	disr	bipart
$\alpha = 0.095$	61%	7%	32%	$\alpha = 0.569$	0%	21%	79%
$\beta = 0.705$	0%	0%	100%	$\beta = 0.477$	0%	5%	95%
$\lambda = 2.106$	0%	1%	99%	$\lambda = 1.581$	3%	26%	71%
$area = 69.78$	4%	31%	65%	$area = 64.52$	31%	57%	12%
avg	16.25%	9.75%	**74%**	**avg**	8.5%	27.25%	**64.25**%

The invasion and conversion of spiral arteries in the maternal uterus by the placentally-derived extravillous trophoblast has been likened to invasion and growth of malignant tumours [3, 13]. Interestingly, this is another area where mathematical modelling has been used to understand the interplay between vascularisation and consequent tumour growth to produce a powerful tool that can explain the in vivo dynamics of tumours [34]. Extension of our mathematical model to include the conversion of maternal vasculature by extravillous trophoblast may provide further understanding of the critical events in early pregnancy which determine placental size, shape and ultimately pregnancy outcome. With advances in ultrasound (and other) imaging more detailed in vivo data, such as direct imaging of spiral arteries in early pregnancy[10] will become available, which can be added to the model. With accurate data from early pregnancy, it may ultimately be possible to predict placental shape, size and vascularisation by a placental model. Such a strategy would have clinical utility in identifying pregnancies that may be at greatest risk of complications.

This work arose from a problem considered at a Mathematics-in-Medicine Study Group[18]. The Study Group and a subsequent follow-up meeting were funded by the Engineering and Physical Sciences Research Council (EP/H00162X/1), and hosted by OCCAM, Mathematical Institute, University of Oxford, UK, with institutional support RVO:68407700

for VK. Thanks to all participating members of the workshop for their input; T. Junaid, M. Kritz, K. Preedy, I. Pu, A. Setchi, J. Siggers, G. Stevenson and R. Whittaker.

This publication was based on work supported in part by Award No KUK-C1-013-04, made by King Abdullah University of Science and Technology (KAUST).

References

[1] D. Barker, K. Thornburg, C. Osmond, E. Kajantie, J. Eriksson, et al. The surface area of the placenta and hypertension in the offspring in later life. *International Journal of Developmental Biology*, 54(2):525, 2010.

[2] M. Berman and H. Cohen, editors. *Diagnostic Medical Sonography: Obstetrics and gynecology*, volume 1. Lippincott Williams & Wilkins, 1997.

[3] W. Billington et al. Biology of the trophoblast. *Advances in reproductive physiology*, 5:27, 1971.

[4] T. Birdsey, R. Boyd, C. Sibley, and S. Greenwood. Microvillous membrane potential (e m) in villi from first trimester human placenta: comparison toe m at term. *American Journal of Physiology-Regulatory, Integrative and Comparative Physiology*, 273(4):R1519–R1528, 1997.

[5] S. Biswas and S. Ghosh. Gross morphological changes of placentas associated with intrauterine growth restriction of fetuses: A case control study. *Early human development*, 84(6):357–362, 2008.

[6] S. Biswas, S. Ghosh, and S. Chhabra. Surface area of chorionic villi of placentas: An index of intrauterine growth restriction of fetuses. *Journal of Obstetrics and Gynaecology Research*, 34(4):487–493, 2008.

[7] P. Callen. *Ultrasonography in Obstetrics and Gynecology*. Saunders, 1994.

[8] I. Chernyavsky, O. Jensen, and L. Leach. A mathematical model of intervillous blood flow in the human placentone. *Placenta*, 31(3):44–52, 2010.

[9] I. Chernyavsky, O. Jensen, and L. Leach. A mathematical model of intervillous blood flow in the human placentone. *Placenta*, 31(1):44–52, 2010.

[10] S. Collins, G. Stevenson, J. Noble, and L. Impey. Developmental changes in spiral artery blood flow in the human placenta observed with colour doppler ultrasonography. *Placenta*, 2012.

[11] J. Eriksson, E. Kajantie, K. Thornburg, C. Osmond, and D. Barker. Mother's body size and placental size predict coronary heart disease in men. *European Heart Journal*, 32(18):2297–2303, 2011.

[12] S. Esmaelzadeh, N. Rezaei, M. HajiAhmadi, et al. Normal uterine size in women of reproductive age in Northern Islamic Republic of Iran. *Eastern Mediterranean Health Journal*, 10(3):437, 2004.

[13] C. Ferretti, L. Bruni, V. Dangles-Marie, A. Pecking, and D. Bellet. Molecular circuits shared by placental and cancer cells, and their implications in the proliferative, invasive and migratory capacities of trophoblasts. *Human reproduction update*, 13(2):121–141, 2007.

[14] J. Gill, C. Salafia, D. Grebenkov, and D. Vvedensky. Modeling oxygen transport in human placental terminal villi. *Journal of Theoretical Biology*, 291:33–41, 2011.

[15] Z. Gordon, O. Eytan, A. Jaffa, and D. Elad. Fetal blood flow in branching models of the chorionic arterial vasculature. *Annals of the New York Academy of Sciences*, 1101(1):250–265, 2007.

[16] C. Guiot, P. Pianta, and T. Todros. Modelling the feto-placental circulation: I. a distributed network predicting umbilical haemodynamics throughout pregnancy. *Ultrasound in Medicine & Biology*, 18(6):535 – 544, 1992.

[17] A. Heazell, S. Collins, S. Cotter, L. Kimpton, T. Junaid, V. Klika, M. Kritz, K. Preedy, I. Pu, A. Setchi, J. Siggers, G. Stevenson, and R. Whittaker. Clinically significant quantitative measures of placental size and shape, cord insertion point, and fetal-placental vascularisation. To be submitted 2013.

[18] A. Heazell, S. Cotter, L. Gallimore, D. Greenhalgh, S. Kennedy, V. Klika, M. Kritz, P. Nielsen, K. Preedy, I. Pu, et al. Comparing placentas from normal and abnormal pregnancies. *Proceedings of the 2010 UK Mathematics-in-Medicine Study Group.*, 2010.

[19] A. Kido, M. Kataoka, T. Koyama, A. Yamamoto, T. Saga, and K. Togashi. Changes in apparent diffusion coefficients in the normal uterus during different phases of the menstrual cycle. *British Journal of Radiology*, 83(990):524–528, 2010.

[20] M. Klamkin. Elementary approximations to the area of n-dimensional ellipsoids. *American Mathematical Monthly*, pages 280–283, 1971.

[21] P. Kloeden and E. Platen. *Numerical solution of stochastic differential equations*, volume 23. Springer, 2011.

[22] O. Luria, J. Bar, M. Kovo, A. Golan, and O. Barnea. Feto-maternal interaction: A mathematical model simulating placental response in hypertensive disorders of pregnancy. *Reproductive Sciences*, 17(10):963–969, 2010.

[23] K. Mardi and J. Sharma. Histopathological evaluation of placentas in IUGR pregnancies. *Indian journal of pathology & microbiology*, 46(4):551–554, October 2003.

[24] J. Meekins, R. Pijnenborg, M. Hanssens, I. MCFadyen, and A. van Asshe. A study of placental bed spiral arteries and trophoblast invasion in normal and severe pre-eclamptic pregnancies. *BJOG: An International Journal of Obstetrics & Gynaecology*, 101(8):669–674, 1994.

[25] G. Milstein. *Numerical integration of stochastic differential equations*, volume 313. Springer, 1994.

[26] K. Page. *The Physiology of the Human Placenta*, chapter 1, page 10. London: University College London Press, 1993.

[27] S. Pathak, E. Hook, G. Hackett, E. Murdoch, N. Sebire, F. Jessop, and C. Lees. Cord coiling, umbilical cord insertion and placental shape in an unselected cohort delivering at term: Relationship with common obstetric outcomes. *Placenta*, 31(11):963–968, 2010.

[28] R. Pijnenborg, L. Vercruysse, and M. Hanssens. The uterine spiral arteries in human pregnancy: facts and controversies. *Placenta*, 27(9):939–958, 2006.

[29] C. Salafia, M. Yampolsky, A. Shlakhter, D. Mandel, and N. Schwartz. Variety in placental shape: when does it originate? *Placenta*, 33(3):164–170, 2012.

[30] R. Sanders and T. Winter. *Clinical sonography: a practical guide*. Lippincott Williams & Wilkins, 1991.

[31] N. Sebire, V. Jain, and D. Talbert. Spiral artery associated restricted growth (SPAARG): a computer model of pathophysiology resulting from low intervillous pressure having fetal programming implications. *Pathophysiology*, 11(2):87–94, 2004.

[32] B. Sengers, C. Please, and R. Lewis. Computational modelling of amino acid transfer interactions in the placenta. *Experimental physiology*, 95(7):829–840, 2010.

[33] T. Sherman. On connecting large vessels to small. the meaning of murray's law. *The Journal of general physiology*, 78(4):431–453, 1981.

[34] K. Swanson, R. Rockne, J. Claridge, M. Chaplain, E. Alvord Jr, and A. Anderson. Quantifying the role of angiogenesis in malignant progression of gliomas: in silico modeling integrates imaging and histology. *Cancer research*, 71(24):7366–7375, 2011.

[35] J. van den Wijngaard, B. Westerhof, M. Ross, and M. Van Gemert. A mathematical model of twin-twin transfusion syndrome with pulsatile arterial circulations. *American Journal of Physiology-Regulatory, Integrative and Comparative Physiology*, 292(4):R1519–R1531, 2007.

[36] W. Warwick and D. Banister. *Gray's anatomy*. Churchill Livingstone, 1989.

[37] M. Yampolsky, C. Salafia, O. Shlakhter, D. Haas, B. Eucker, and J. Thorp. Modeling the variability of shapes of a human placenta. *Placenta*, 29(9):790 – 797, 2008.

[38] M. Yampolsky, C. Salafia, O. Shlakhter, D. Haas, B. Eucker, and J. Thorp. Centrality of the umbilical cord insertion in a human placenta influences the placental efficiency. *Placenta*, 30(12):1058–1064, 2009.

RECENT REPORTS

12/107	Coalescence of Liquid Drops: Different Models Versus Experiment	Sprittles Shikhmurzaev
12/108	Adjoint Based A Posteriori Analysis of Multiscale Mortar Discretizations with Multinumerics	Tavener Wildey
12/109	Dynamics of mechanically induced fiber reorientation in the material reinforced by two families of fibers	Melnik Goriely
12/110	Multiscale stochastic reaction-diffusion modelling: application to actin dynamics in filopodia	Erban Flegg Papoian
12/111	Exploiting the Synergy Between Carboplatin and ABT-737 in the Treatment of Ovarian Carcinomas	Jain Richardson Meyer-Hermann Byrne
12/112	The integration of hormonal signaling networks and mobile microRNAs is required for vascular patterning in Arabidopsis roots	Muraro Pound Help Lucas Chopard Byrne Godin Hodgman King Pridmore Helariutta Bennett Bishopp
12/113	Fast solution of Cahn-Hilliard Variational Inequalities using Implicit Time Discretization and Finite Elements	Bosch Stoll Benner
12/114	An Embedding Technique for the Solution of Reaction-Diffusion Equations on Algebraic Surfaces with Isolated Singularities	Rockstroh März Ruuth
12/115	Mathematicians at the Movies: Sherlock Holmes vs. Professor Moriarty	Moulton Goriely
13/01	Rotation, inversion, and perversion in anisotropic elastic cylindrical tubes and membranes	Goriely Tabor
13/02	Drop spreading and penetration into pre-wetted powders	Marston Sprittles Zhu Li Vakarelski Thoroddsen
13/03	On the mechanics of thin films and growing surfaces	Holland Kosmata Goriely Kuhl

13/06	A Volume-Based Method for Denoising on Curved Surfaces	Biddle von Glehn Macdonald März
13/07	Porous squeeze-film flow	Knox Wilson Duffy McKee
13/08	Diffusion of finite-size particles in confined geometries	Bruna Chapman
13/09	Mathematical analysis of a model for the growth of the bovine corpus luteum	Prokopiou Byrne Jeffrey Robinson Mann Owen
13/10	Capillary deformations of bendable films	Schroll Adda-Bedia Cerda Huang Menon Russell Toga Vella Davidovitch
13/11	Twist and stretch of helices: All you need is Love	Đuričković Goriely Maddocks
13/12	Switch on, switch off: stiction in nanoelectromechanical switches	Wagner Vella
13/13	Pinning, de-pinning and re-pinning of a slowly varying rivulet	Paterson Wilson Duffy
13/14	Travelling-wave similarity solutions for a steadily translating slender dry patch in a thin fluid film	Yatim Duffy Wilson

Copies of these, and any other OCCAM reports can be obtained from:

Oxford Centre for Collaborative Applied Mathematics
Mathematical Institute

24 - 29 St Giles'
Oxford
OX1 3LB
England
www.maths.ox.ac.uk/occam